Electronic Supplementary Information

Gradient aligned Au/graphene meshes with confined heat at multiple levels for solar evaporation and anti-gravity catalytic conversion

Xiangyu Meng,[a] Jianhui Yang,[a] Seeram Ramakrishna,[b] Yueming Sun[a] and Yunqian Dai*[,a]

[a] *School of Chemistry and Chemical Engineering, Southeast University, Nanjing, Jiangsu 211189, P. R. China*

[b] *Center for Nanofibers and Nanotechnology, Department of Mechanical Engineering, National University of Singapore, Singapore 117574, Singapore*

[*] *Address corresponding to: daiy@seu.edu.cn*

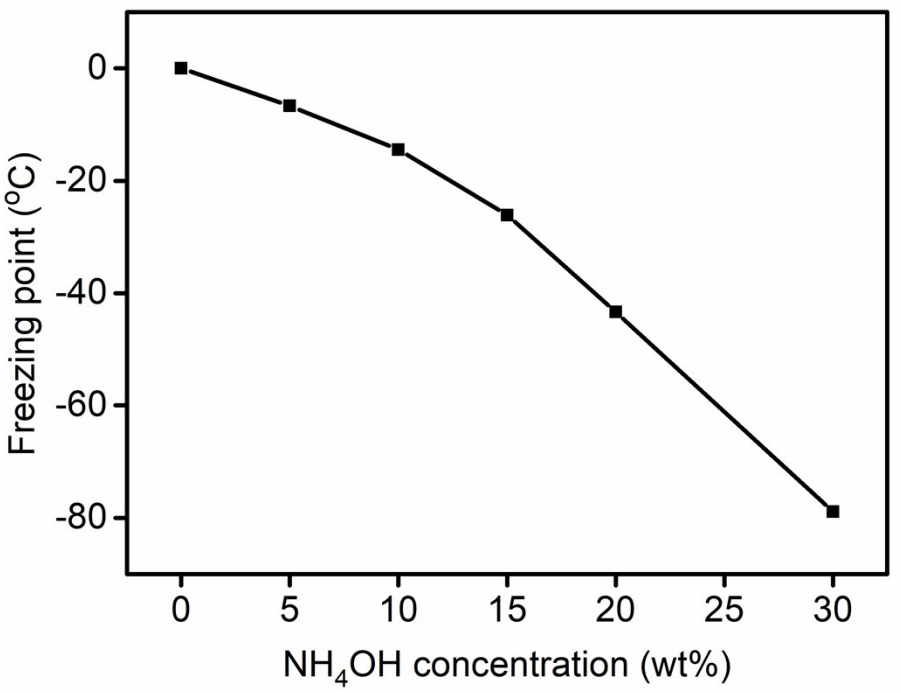

Fig. S1 Relationship curve between typical NH_4OH concentrations and freezing points.

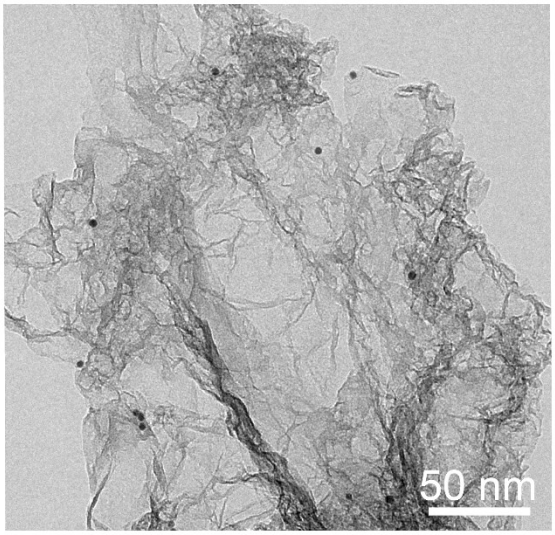

Fig. S2 TEM image of Au/N-RGO mesh taken from the aerogel.

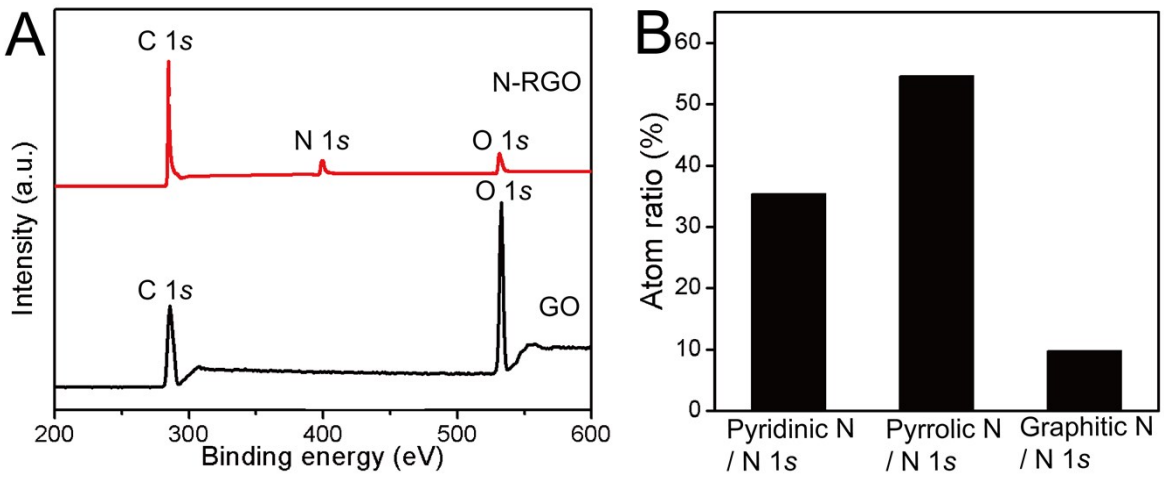

Fig. S3 (A) Full XPS spectra of N-RGO aerogel and pristine GO. (B) The peak area ratio of pyridinic N, pyrrolic N and graphitic N to all N 1*s*.

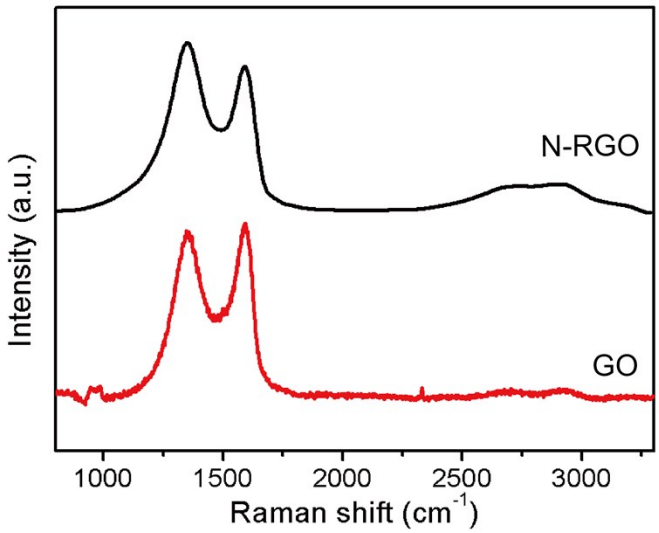

Fig. S4 Raman spectra of N-RGO aerogel and pristine GO.

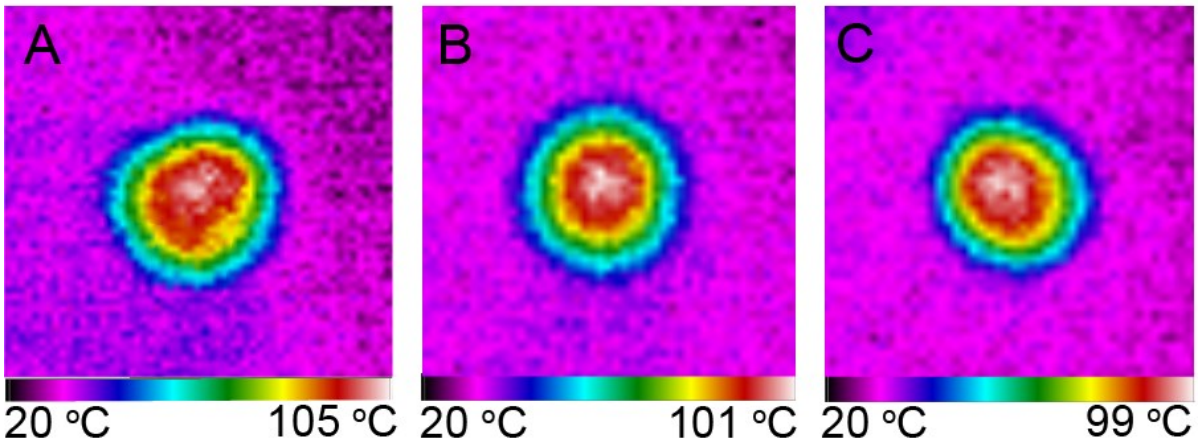

Fig. S5 Comparison of infrared image recorded the temperature of ring-like Au/N-RGO (A) with gradient (B) with uniform and small-sized channels, and (C) with uniform and large-sized channels after light irradiation (2 $kW \cdot m^{-2}$) for 1 hour.

Supplementary Note

Note S1. The calculation of photothermal conversion efficiency.

Notably, as the temperature reaches equilibrium, the input thermal energy converted from light, is regarded as equal to the heat flowing among the exposed surface of Au/N-RGO aerogel and the surrounding. Herein, the photothermal conversion efficiency (E) can be calculated from equation S1:[1]

$$E = \frac{h \cdot (T2 - T1)}{\rho L} \tag{1}$$

where h is the convection heat transfer coefficient ($W \cdot m^{-2} \cdot K^{-1}$), T_2 and T_1 are the weighted average temperatures of Au/N-RGO aerogel after and before light irradiation (K), respectively. The temperature was recorded from infrared images. ρ_L is the light power density ($W \cdot m^{-2}$). In this work, h = 25 $W \cdot m^{-2} \cdot K^{-1}$, ρ_L = 2 $kW \cdot m^{-2}$.

Table S1. Comparison of the photothermal conversion efficiency.

Materials	Photothermal conversion efficiency (%)	Light intensity ($kW \cdot m^{-2}$)	Reference
Gradient ring-like Au/N-RGO	80.0	2	This work
Oxygen plasma treated graphene	53.5	3	[2]
Hierarchical graphene	69.2	3	[3]
Carbonized mushroom	42.5	1	[4]
Nickel/Cobalt/Polydopamine	32.2	1	[5]
Au/Polyacrylonitrile	30.0	1	[6]
Hydroxyapatite/Polydopamine/Chitosan	60.0	1	[7]

Data were given or calculated in the respective references.

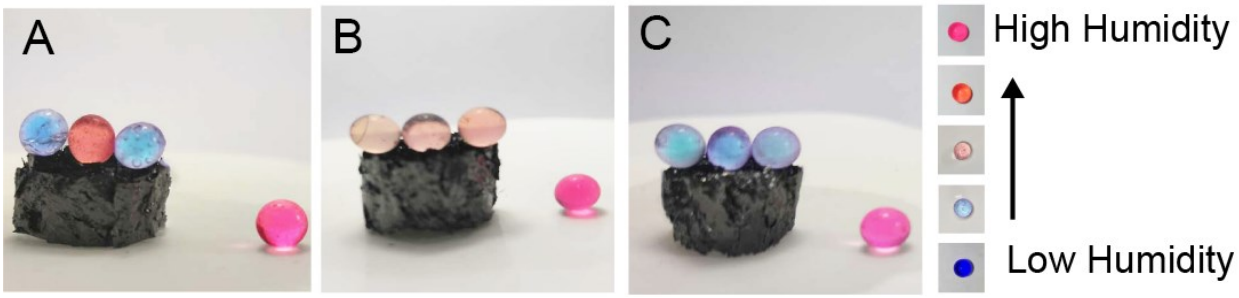

Fig. S6 Concentrated water pumping in the center of (A) the ring-like Au/N-RGO aerogel with gradient microchannels, which was not observed in (B) the ring-like Au/N-RGO aerogel with uniform and small-sized microchannels, or (C) the ring-like Au/N-RGO aerogel with uniform and large-sized microchannels. The right inset showed the color reference images of anhydrous silicon spheres under different relative humidity conditions.

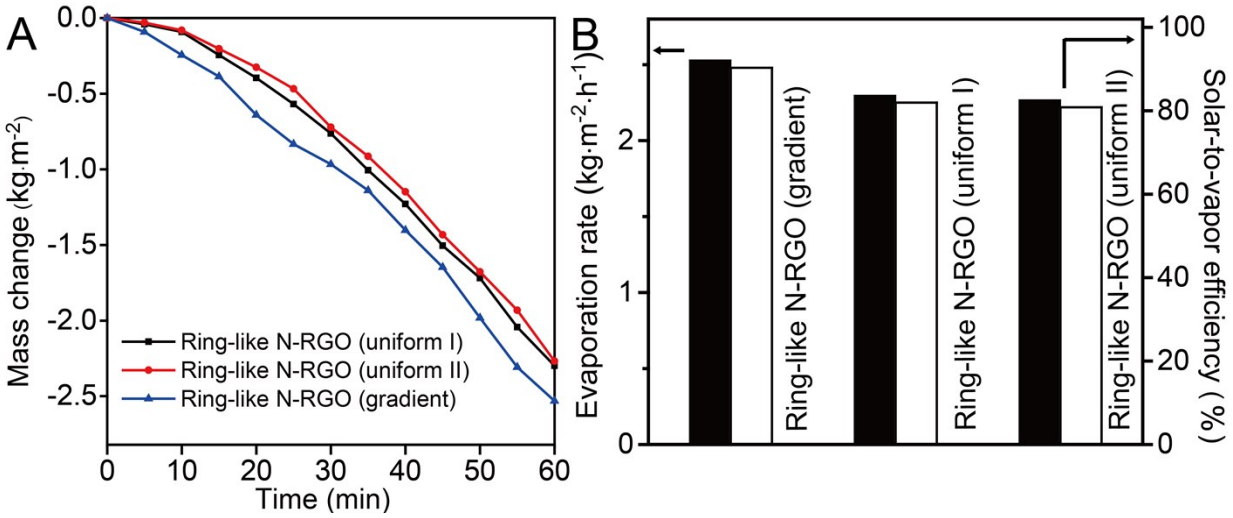

Fig. S7 The mass change as a function of evaporation time, (B) the evaporation rate (black bar) and the solar-to-vapor conversion efficiency (white bar) of ring-like N-RGO aerogels with or without gradient. "Gradient" represented gradient channels, "uniform I" represented the uniform and small-sized channels, "uniform II" represented the uniform and large-sized channels.

Note S2. The calculation of energy gained from environment.

As shown in Fig. S3, the exposed side surface had a lower temperature than that of surrounding, which could gain energy from the surrounding. The energy (E) gained from environment can be calculated by the following equation S2:[8]

$$E = -A_{side} \cdot \varepsilon \cdot \sigma \left(T_{side}^4 - T_s^4\right) - A_{side} \cdot h \left(T_{side} - T_s\right) \quad (2)$$

where A_{side} is the side wall surface area, T_{side} is the average temperature of side surface, T_s is the surrounding temperature, ε is emissivity of the graphene absorber, σ is the Stefan–Boltzmann constant, and h is the average convection heat transfer coefficient. In this work, the energy of N-RGO evaporator gained from environment was 30.03 mW.

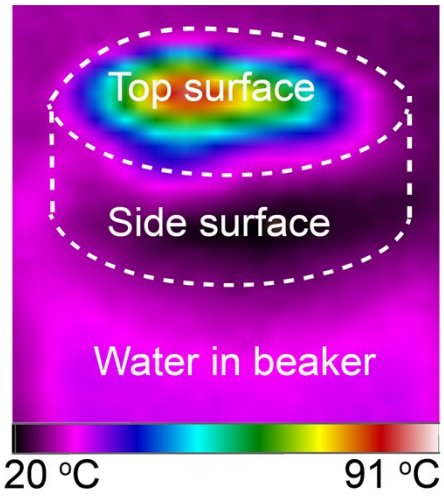

Fig. S8 The infrared image of ring-like Au/N-RGO aerogel during water evaporation. The white circles highlight the boundary lines of different parts.

Table S2. Comparison of the solar-to-vapor conversion efficiency.

Materials	Solar-to-vapor conversion efficiency (%)	Light intensity ($kW \cdot m^{-2}$)	Reference
Gradient ring-like Au/N-RGO	97.1	2	This work
Au/anodized aluminum oxide	57.0	20	[9]
Au/bacterial nanocellulose aerogel	76.3	51	[10]
Ag/PVDF	29.6	23	[11]
Graphene sponge	89.6	1	[12]
3D graphene	87.0	1	[13]
Carbon nanofiber/Carbon nanotube	88.5	2	[14]
Wood/Carbon nanotubes	85.3	2	[15]

PVDF represents the polyvinylidene fluoride. Data were given or calculated in the respective references.

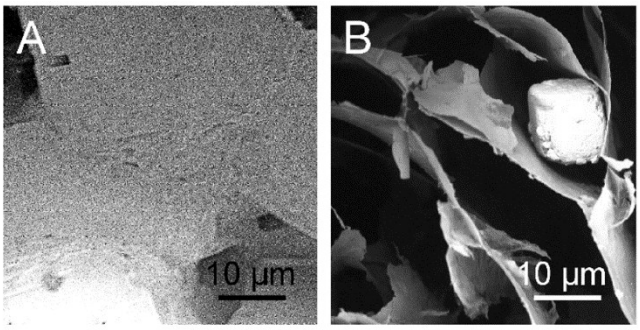

Fig. S9 SEM images showing the change of preplaced NaCl on top surface of (A) honeycomb-like Au/ aerogel and (B) ring-like Au/ N-RGO aerogel after evaporation for one hour.

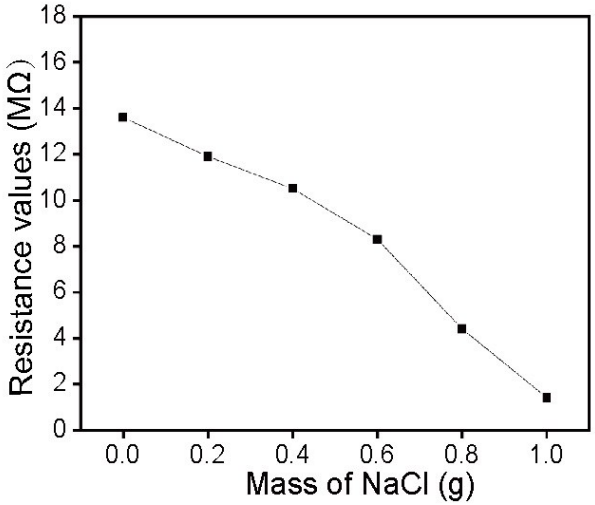

Fig. S10 The relationship between electrical resistance of NaCl aqueous solution against the adding mass of NaCl into the simulated salty water.

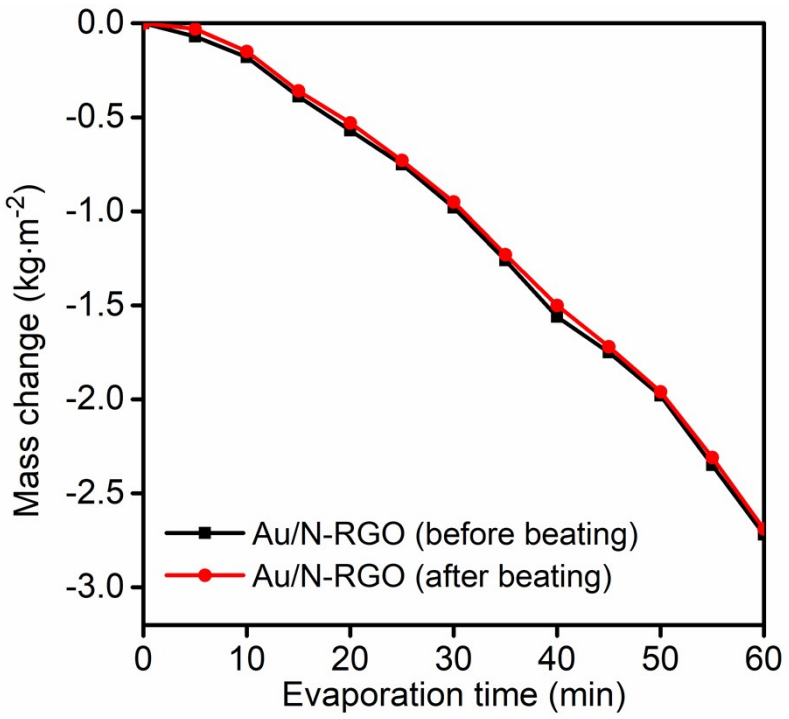

Fig. S11 The mass change as a function of evaporation time, recording the water evaporation performance achieved by gradient ring-like Au/N-RGO aerogels before and after the simulated beating for 30 min.

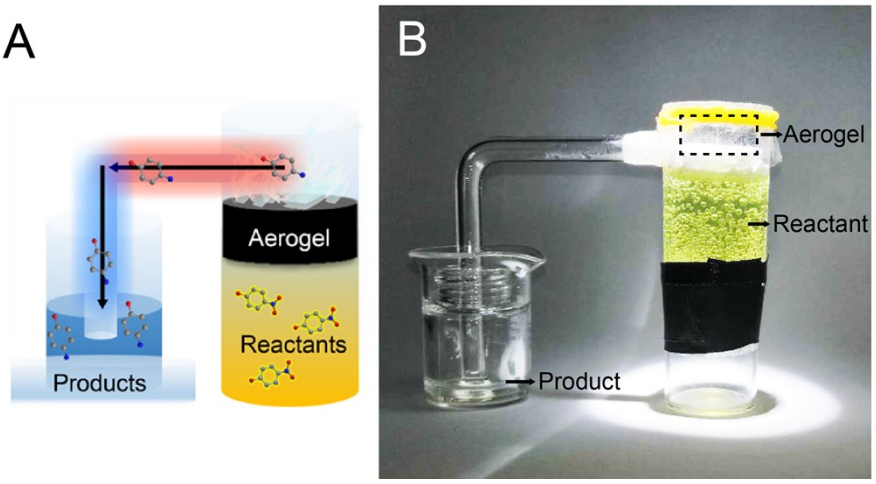

Fig. S12 (A) The schematic illustration and (B) optical image of the setup for self-pumping chemical conversion reaction.

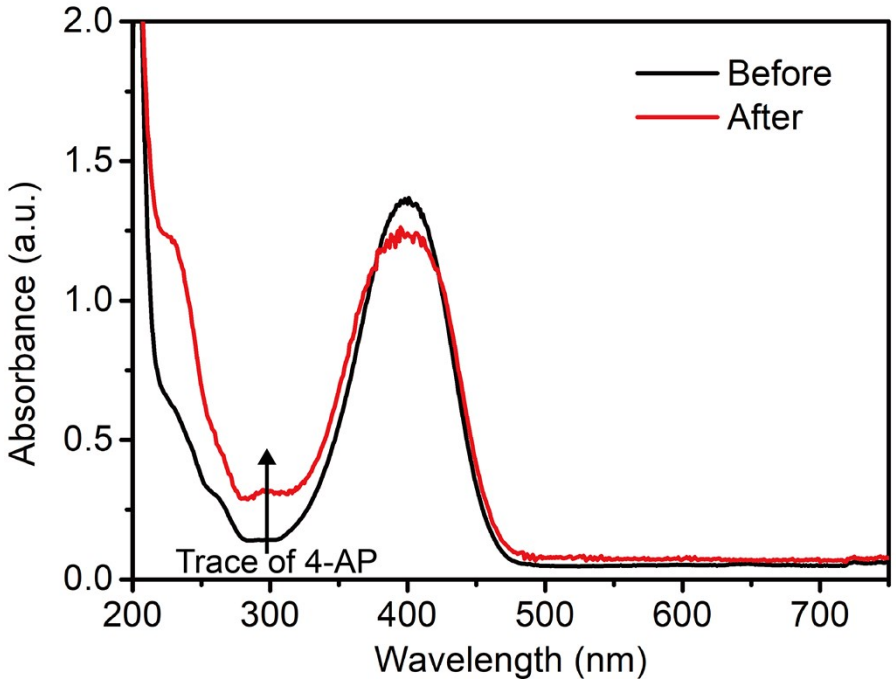

Fig. S13 The comparison of bulky water before and after anti-gravity catalyzing. The arrows highlighted the trace number of 4-aminophenol (4-AP) products.

References

1 M. Weng, P. Zhou, L. Chen, L. Zhang, W. Zhang, Z. Huang, C. Liu and S. Fan, *Adv. Funct. Mater.*, 2016, **26**, 7244–7253.

2 M. Gaboardi, A. Bliersbach, G. Bertoni, M. Aramini, G. Vlahopoulou, D. Pontiroli, P. Mauron, G. Magnani, G. Salviati, A. Züttel and M. Riccò, *J. Mater. Chem. A*, 2014, **2**, 1039−1046.

3 K. Liu, Q. Jiang, S. Tadepalli, R. Raliya, P. Biswas, R. Naik and S. Singamaneni, *ACS Appl. Mater. Interfaces*, 2017, **9**, 7675−7681.

4 N. Xu, X. Hu, W. Xu, X. Li, L. Zhou, S. Zhu and J. Zhu, *Adv. Mater.*, 2017, **29**, 1606762.

5 B. Shao, Y. Wang, X. Wu, Y. Lu, X. Yang, G. Y. Chen, G. Owens and H. Xu, *J. Mater. Chem. A*, 2020, **8**, 11665−11673.

6 Z. Huang, S. Li, X. Cui, Y. Wan, Y. Xiao, S. Tian, H. Wang, X. Li, Q. Zhao and C. S. Lee, *J. Mater. Chem. A*, 2020, **8**, 10742−10746.

7 S. Cao, X. Wu, Y. Zhu, R. Gupta, A. Tan, Z. Wang, Y. S. Jun and S. Singamaneni, *J. Mater. Chem. A*, 2020, **8**, 5147−5156.

8 X. Li, J. Li, J. Lu, N. Xu, C. Chen, X. Min, B. Zhu, H. Li, L. Zhou, S. Zhu, T. Zhang and J. Zhu, *Joule*, 2018, **2**, 1331−1338.

9 K. Bae, G. Kang, S. Cho, W. Park, K. Kim and W. Padilla, *Nat. Commun.*, 2015, **6**, 10103−10111.

10 L. Tian, J. Luan, K. Liu, Q. Jiang, S. Tadepalli, M. Gupta, R. Naik and S. Singamaneni, *Nano Lett.*, 2016, **16**, 609−616.

11 A. Politano, P. Argurio, G. Profio, V. Sanna, A. Cupolillo, S. Chakraborty, H. Arafat and E. Curcio, *Adv. Mater.*, 2017, **29**, 1603504.

12 L. Cui, P. Zhang, Y. Xiao, Y. Liang, H. Liang, Z. Cheng and L. Qu, *Adv. Mater.*, 2018, **30**, 1706805.

13 Y. Yang, R. Zhao, T. Zhang, K. Zhao, P. Xiao, Y. Ma, P. Ajayan, G. Shi and Y. Chen, *ACS Nano*, 2018, **12**, 829−835.

14 H. Ren, M. Tang, B. Guan, K. Wang, J. Yang, F. Wang, M. Wang, J. Shan, Z. Chen, D. Wei, H. Peng and Z. Liu, *Adv. Mater.*, 2017, **29**, 1702590−1702596.

15 F. Jiang, H. Liu, Y. Li, Y. Kuang, X. Xu, C. J. Chen, H. Huang, C. Jia, X, Zhao, E. Hitz, Y. Zhou, R. Yang, L. Cui and L. Hu, *ACS Appl. Mater. Interfaces*, 2018, **10**, 1104–1112.